Journal of Thermal Analysis, Vol. 42 (1994) 667-678

HEAT TREATMENT OF RAPIDLY SOLIDIFIED Fe–Cr–Zr–B ALLOYS

I. T. H. Chang, K. Ishii and B. Cantor*

Oxford Centre for Advanced Materials and Composites, Department of Materials, University of Oxford, Parks Road, Oxford OX1 3PH, UK
*Kawasaki Steel Corporation, 1 Kawasaki-cho, Chiba, Japan

Abstract

The crystallization behaviour of amorphous melt spun $Fe_{82-x-y}Cr_{18}Zr_xB_y$ (x = 0–8, y = 10–20) ribbons have been investigated using differential scanning calorimetry. The crystallization temperature and crystallization behaviour change with varzing Zr and B content.

The microstructural development during annealing of amorphous $Fe_{64}Cr_{18}Zr_8B_{10}$ has been investigated by a combination of transmission electron microscopy and energy dispersive X-ray microanalysis. Isothermal annealing for 2 h at temperatures in the range 600–1000°C produces a variety of different microstructures depending on the annealing temperature. At 600°C, the amorphous alloy partially crystallizes to a form a microstructure consisting of 9 nm sized bcc ferrite grains embedded in an amorphous matrix. At temperatures in the range 700–900°C, the alloy microstructure transforms into a mixture of bcc ferrite, faulted fcc MB_{12} boride particles and tetragonal M_3B boride particles. At 1000°C, the faulted fcc MB_{12} boride particles are replaced by orthorhombic M_4B boride particles.

Keywords: alloys. amorphous, DSC, het treatment, solidification

Introduction

In-situ Fe-based particulate composites have attracted much attention recently, because of their unique properties, such as high strength, excellent thermal stability and superior corrosion and oxidation resistance [1–7]. The composites consist of stable borides embedded in an Fe matrix and are manufactured from Fe–Tm–B alloys (*Tm* = transition metal) by rapid solidification followed by hot consolidation [1–4]. The alloys are fully or partially amorphous after rapid solidification [3–5], and the final microstructures are controlled by amorphous/crystalline and crystalline/crystalline transformations during subsequent annealing and consolidation.

The present work concentrates on differential scanning calorimetry (DSC) and transmission electron microscopy (TEM) studies of the heat treatment of a range of rapidly solidified Fe–Cr–Zr–B quaternary alloys prepared by melt

0368–4466/94/ $ 4.00

John Wiley & Sons, Limited
Chichester

spinning. This paper describes the effects of Zr and B content on the crystallization behaviour, together with a detailed description of the microstructural evolution in melt spun $Fe_{64}Cr_{18}Zr_8B_{10}$ during heat treatment over temperatures in the range 600–1000°C.

Experimental methods

Ribbons of $Fe_{82-x-y}Cr_{18}Zr_xB_y$ (x = 0–8, y = 10–20), 30–50 μm in thickness, were manufactured by chill block melt spinning in air. The crystallization behaviour of the as-melt spun ribbons was studied using a TA Instruments 2000 thermal analyzer/910 DSC. Specimens of melt spun $Fe_{64}Cr_{18}Zr_8B_{10}$ were also annealed for 2 h in sealed quartz tubes filled with Ar gas at different temperatures in the range 600–1000°C, and the resulting microstructures characterized in a Philips CM20 TEM fitted with a Link Systems energy dispersive X-ray microanalyzer (EDX). TEM specimens were prepared by mechanical polishing followed by twin-jet electro-polishing in 73 vol.% ethanol+8 vol.% perchloric acid+10 vol.% butylcellosolve+9 vol.% distilled water at −10 to −15°C.

Results and discussion

Crystallization behaviour of melt spun Fe–Cr–Zr–B

Figures 1 and 2 show typical DSC traces from the melt spun $Fe_{82-x-y}Cr_{18}Zr_xB_y$ (x = 0–8, y = 10–20) alloys obtained during continuous heating to 710°C at a rate of 5 deg·min^{-1}. The continuous heating traces showed

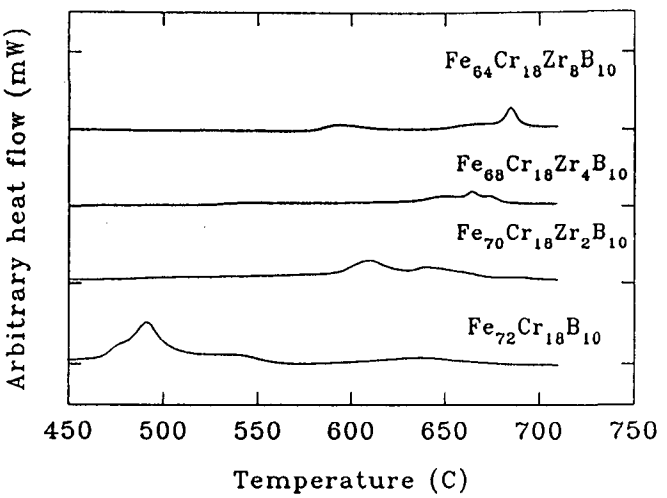

Fig. 1 DSC traces of melt spun $Fe_{72-x}Cr_{18}Zr_xB_{10}$ alloys (x = 0–8)

several exothermic peaks. The strongest exothermic peak in the ternary $Fe_{72}Cr_{18}B_{10}$ base alloy was at 419°C. With increasing Zr content, the strongest exothermic peak temperature increased to 609, 665 and then 685°C, corresponding to 2, 4 and 8 at.% Zr, as shown in Fig. 1. However, the primary exothermic peak decreased from 609°C for $Fe_{70}Cr_{18}Zr_2B_{10}$ to 550°C for

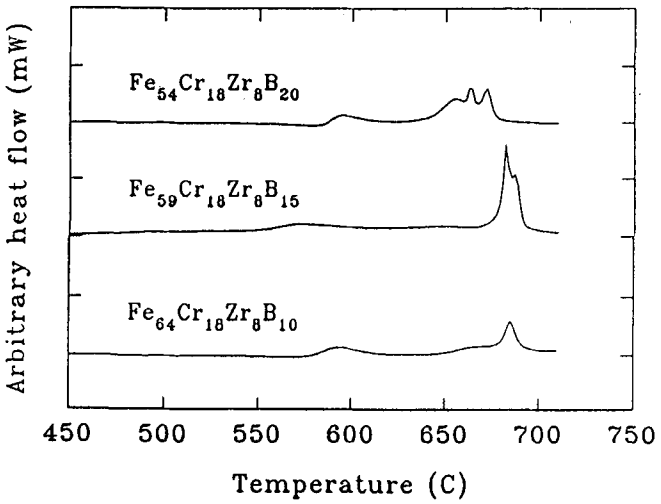

Fig. 2 DSC traces of melt spun $Fe_{74-y}Cr_{18}Zr_8B_y$ alloys (y = 10–20)

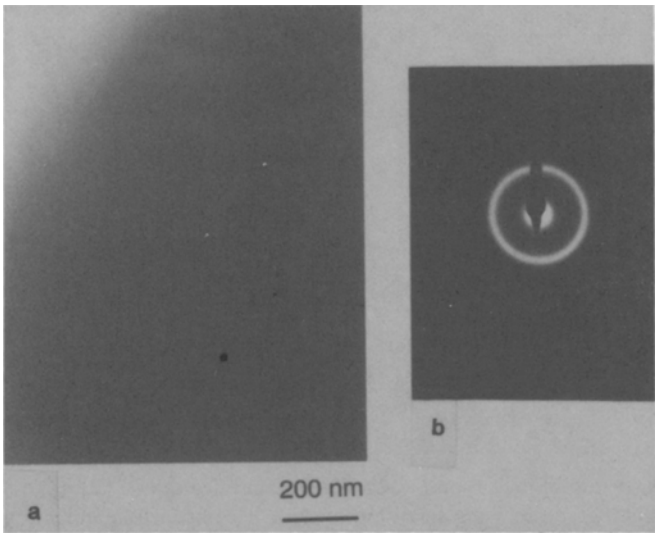

Fig. 3 (a) Bright field TEM micrograph of as-melt spun $Fe_{64}Cr_{18}Zr_8B_{10}$ and (b) corresponding SADP showing amorphous halo rings

$Fe_{68}Cr_{18}Zr_4B_{10}$ and then increased to 590°C for $Fe_{64}Cr_{18}Zr_8B_{10}$. With increasing B content, the crystallization behaviour changed from two exothermic peaks for $Fe_{64}Cr_{18}Zr_8B_{10}$ to three for $Fe_{59}Cr_{18}Zr_8B_{15}$ and then to four for $Fe_{54}Cr_{18}Zr_8B_{20}$, as shown in Fig. 2. In general, the crystallization temperatures of the Fe–Cr–Zr–B alloys were higher than previous measurements for an $Fe_{70}Cr_{18}Mo_2B_{10}$ alloy [4].

Microstructural evolution in heat treated $Fe_{64}Cr_{18}Zr_8B_{10}$

Figures 3(a) and (b) show respectively a bright field TEM micrograph and a corresponding selected area diffraction pattern (SADP) from as-melt spun $Fe_{64}Cr_{18}Zr_8B_{10}$. The as-melt spun alloy consisted of a fully amorphous structure with no contrast in the micrograph and amorphous halo rings in the SADP.

After annealing for 2 h at 600°C, amorphous $Fe_{64}Cr_{18}Zr_8B_{10}$ became partially crystallized. Figures 4(a) and (b) show respectively a bright field TEM micrograph and a corresponding SADP from the annealed ribbon. The annealed

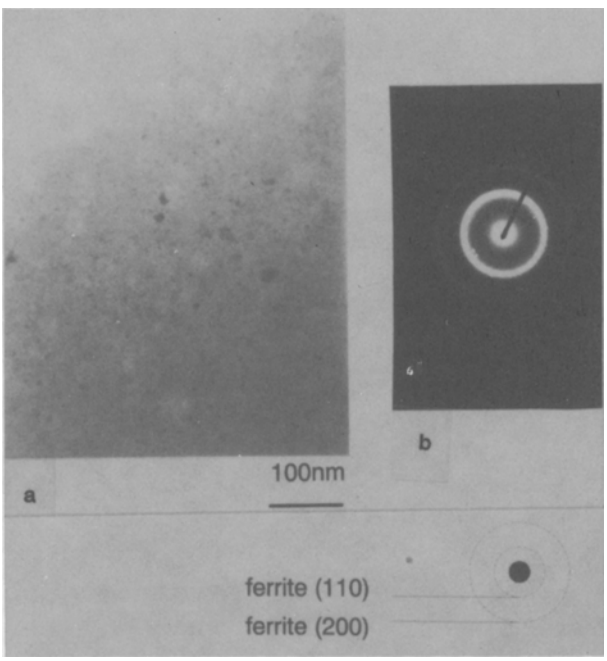

Fig. 4 Microstructure of melt spun $Fe_{64}Cr_{18}Zr_8B_{10}$ annealed at 600°C for 2 h: (a) bright field TEM micrograph showing small ferrite crystals embedded in an amorphous matrix; and (b) corresponding SADP showing amorphous halo rings from the amorphous matrix together with a few diffraction spots from the small ferrite crystals

microstructure consisted of 9 nm sized crystals embedded in an amorphous matrix, as shown in Fig. 4(a). The crystals were identified as body centred cubic (bcc) ferrite from the SADP, which consisted of a polycrystalline bcc ring pattern superimposed on amorphous halo rings, as shown in Fig. 4(b).

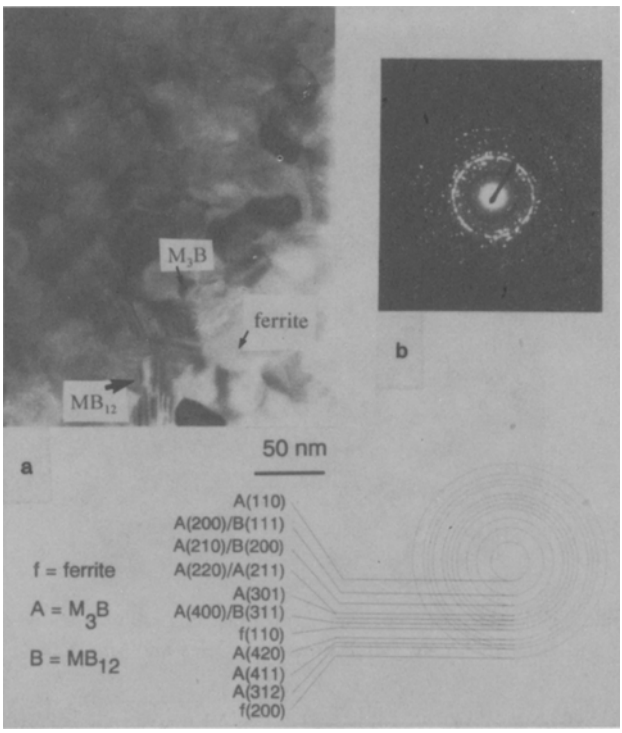

Fig. 5 Microstructure of melt spun $Fe_{64}Cr_{18}Zr_8B_{10}$ annealed at 700°C for 2 h: (a) bright field TEM micrograph showing a mixture of ferrite, $M_{12}B$ boride particles and M_3B boride particles; and (b) corresponding SADP showing polycrystalline ring pattern

At higher annealing temperatures in the range 700–900°C, amorphous $Fe_{64}Cr_{18}Zr_8B_{10}$ crystallized fully. Figures 5–7 show typical bright field TEM micrographs and corresponding SADPs from ribbons annealed at 700, 800 and 900°C respectively, in each case consisting of a mixture of bcc ferrite, face centred cubic (fcc) MB_{12} boride particles and tetragonal M_3B boride particles. The lattice constant of fcc MB_{12} was $a = 0.741$ nm and the lattice constants of tetragonal M_3B were $a = 0.861$ nm and $c = 0.431$ nm. The MB_{12} boride contained internal (111) twins, which produced the fringe contrast in the particles as shown in Figs 5–7. The ferrite grains, fcc MB_{12} boride particles and tetrago-

nal M_3B boride particles all increased in size, from 50 to 405 nm, 38 to 200 nm and 12 to 67 nm respectively, as the annealing temperature increased from 700 to 900°C.

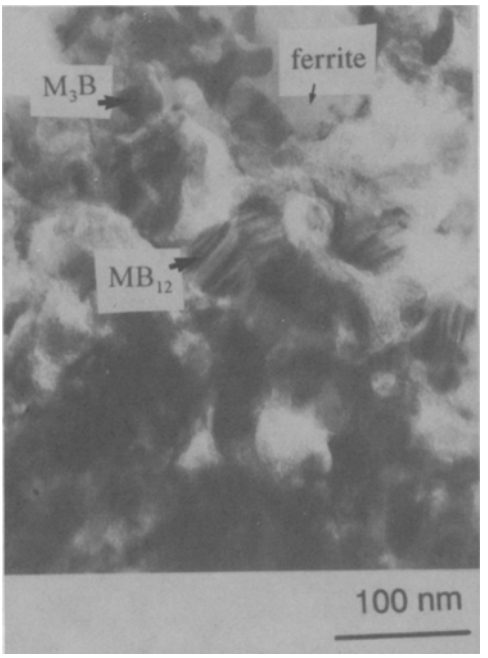

Fig. 6 Bright field TEM micrograph of melt spun $Fe_{64}Cr_{18}Zr_8B_{10}$ annealed at 800°C for 2 h showing a mixture of ferrite, $M_{12}B$ boride particles and M_3B boride particles

Figures 8(a)–(c) show typical EDX traces from the bcc ferrite, fcc MB_{12} and tetragonal M_3B respectively, after annealing at 900°C for 2 h. The ferrite grains contained Fe, Cr and a very low Zr content, giving an average composition of 75Fe–24Cr–1Zr (at.%). The MB_{12} boride particles contained Fe, Cr and Zr, giving an average composition of 64Fe–10Cr–26Zr (at.%). The M_3B boride particles were mostly Zr with relatively low Fe and Cr content, giving an average composition of 28Fe–9Cr–63Zr (at.%).

After annealing at for 2 h at 1000°C, the $Fe_{64}Cr_{18}Zr_8B_{10}$ transformed further. Figures 9(a)–(d) show a typical bright field TEM micrograph and corresponding SADPs from the annealed ribbon. The annealed microstructure consisted of a mixture of orthorhombic M_4B boride particles and tetragonal M_3B boride particles embedded in a ferrite matrix. The lattice constants of M_4B were $a = 1.458$ nm, $b = 0.738$ nm and $c = 0.425$ nm. Figures 10(a)–(c) show typical EDX traces from the bcc ferrite, orthorhombic M_4B and tetragonal M_3B

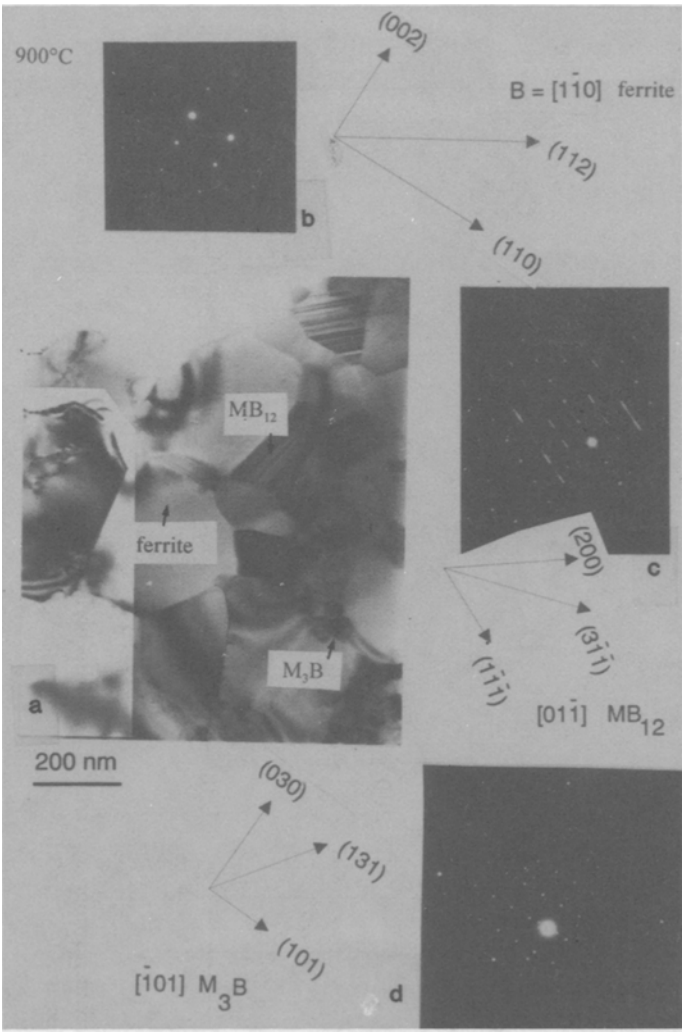

Fig. 7 Microstructure of melt spun $Fe_{64}Cr_{18}Zr_8B_{10}$ annealed at 900°C for 2 h: (a) bright field TEM micrograph showing a mixture of ferrite, $M_{12}B$ boride particles and M_3B boride particles; and (b)–(d) corresponding SADPs from ferrite, an $M_{12}B$ boride particle and an M_3B boride particle respectively

respectively. The ferrite grains contained Fe, Cr and a very low Zr content, giving and average composition of 73Fe–26Cr–1Zr (at.%), similar to the composition after annealing at 900°C as shown in Fig. 8(a). The M_4B boride particles contained Fe, Cr and Zr, giving an average composition of 40Fe–14Cr–46Zr (at.%). The M_3B boride particles contained mostly Zr with relatively low Fe

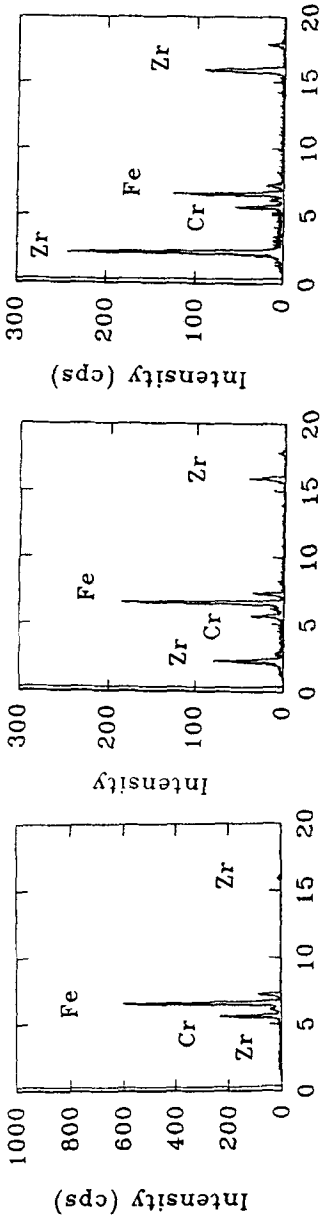

Fig. 8 Energy dispersive X-ray traces from (a) ferrite, (b) an MB_{12} boride particle, and (c) an M_3B boride particle in melt spun $Fe_{64}Cr_{18}Zr_8B_{10}$ annealed at 900°C for 2 h

and Cr contents, giving an average composition of 21Fe–10Cr–69Zr (at.%), again similar to the composition after annealing at 900°C as shown in Fig. 8(c).

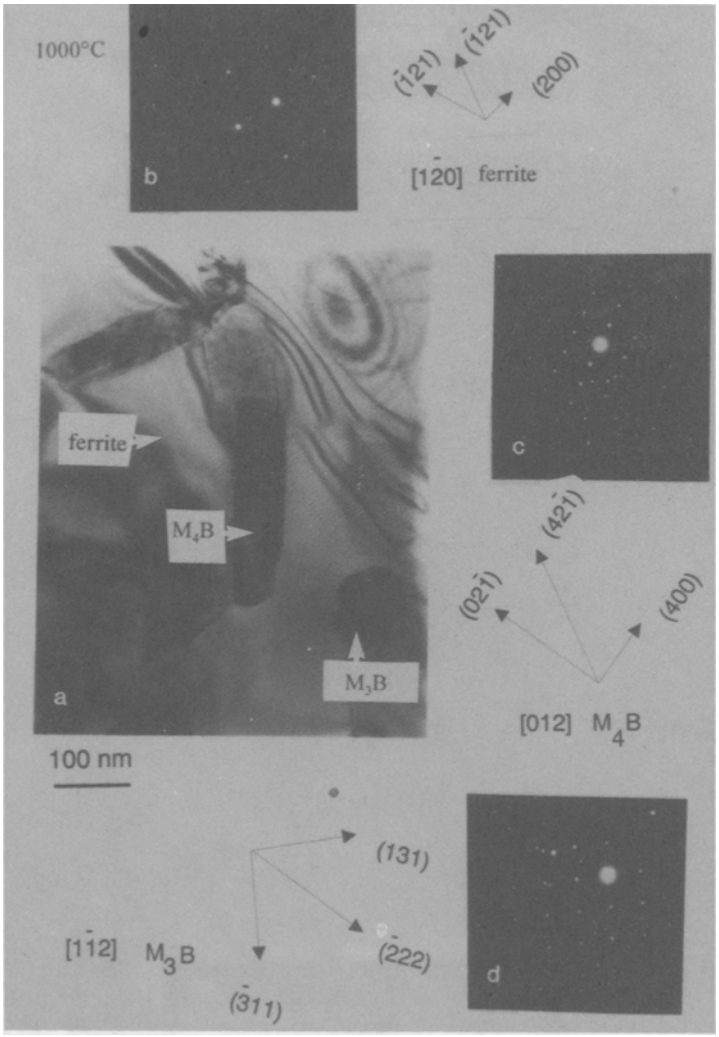

Fig. 9 Microstructure of melt spun $Fe_{64}Cr_{18}Zr_8B_{10}$ annealed at 1000°C for 2 h: (a) bright field TEM micrograph showing a mixture of ferrite, M_4B boride particles and M_3B boride particles; and (b)–(d) corresponding SADPs from ferrite, an M_4B boride particle and an M_3B boride particle respectively

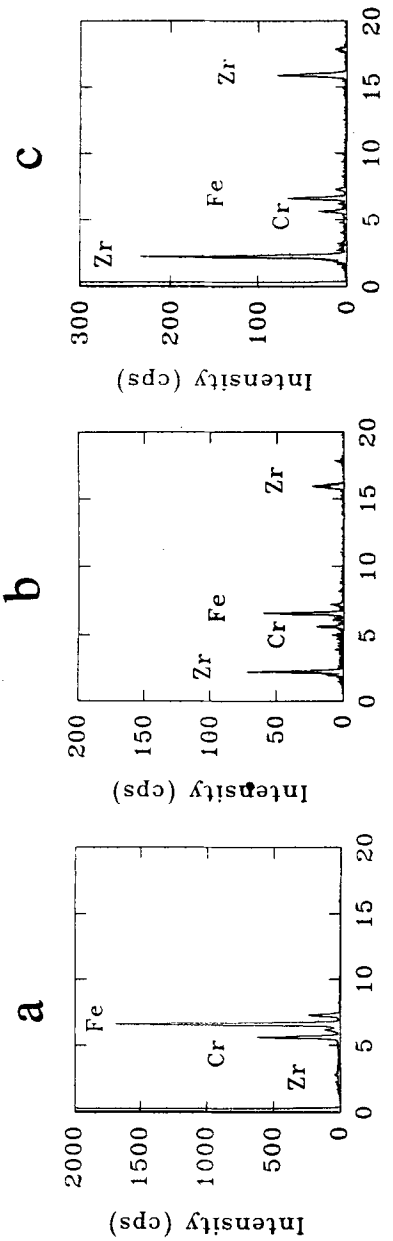

Fig. 10 Energy dispersive X-ray traces from (a) ferrite, (b) an M_4B boride particle, and (c) an M_3B boride particle in melt spun $Fe_{64}Cr_{18}Zr_8B_{10}$ annealed at 1000°C for 2 h

Conclusions

For amorphous melt spun $Fe_{82-x-y}Cr_{18}Zr_xB_y$ (x = 0–8, y = 10–20) ribbons, the strongest exothermic peak temperature increases with increasing Zr content and the crystallization behaviour becomes more complex with increasing B content. The primary exothermic peak corresponds to the crystallization of ferrite and subsequent peaks correspond to the formation of different borides.

The following transformations take place when amorphous $Fe_{64}Cr_{18}Zr_8B_{10}$ is annealed for 2 h at temperatures in the range 600–1000°C:

(1) amorphous → amorphous + ferrite (600°C)

(2) amorphous + ferrite → ferrite + MB_{12} + M_3B (700–900°C)

(3) ferrite + MB_{12} + M_3B → ferrite + M_4B + M_3B (1000°C)

* * *

We would like to thank Professor R. J. Brook for providing laboratory facilities, the UK Science & Engineering Research Council and Kawasaki Steel for financial support, and Dr. W. T. Kim for helpful discussions.

References

1 R. Ray, in B. H. Kear, B. C. Giessen and M. Cohen (eds.), Rapidly Solidified Amorphous and Crystalline Alloys, North-Holland, Amsterdam 1982, p. 435.
2 M. J. Rawson, D. J. Manley, H. A. Davies and J. E. Restall, in P. W. Lee and J. H. Mole (eds), Rapidly Solidified Materials – Properties and Processing, edited by, American Society for Metals, Metals Park, OH, 1988, p. 37.
3 W. T. Kim, B. Cantor, K. Clay and C. Small, in P. K. Liau and M. N. Gungor (eds), Fundamental Relationships Between Microstructure and Mechanical Properties of Metal Matrix Composites, TMS, Warrendale, PA, 1990, p. 89.
4 W. T. Kim, K. Clay, C. Small and B. Cantor, J. Non-crystalline Solids, 127 (1991) 273.
5 S. Hahn, S. Isserow and R. Ray, J. Mater. Sci,. 22 (1987) 3396.
6 R. Ray, V. Panchanathan and S. Isserrow, J. Metals, 35 (1983) 30.
7 S. Hahn, S. Isserow and R. Ray, J. Mater. Sci. Letters, 4 (1985) 972.

Zusammenfassung — Mittels DSC wurde das Kristallisationsverhalten von amorphen schmelzgesponnenen Bändern aus $Fe_{82-x-y}Cr_{18}Zr_xB_y$ (x = 0.8, y = 10–20) untersucht. Die Kristallisationstemperatur steigt mit zunehmenden Zr-Gehalt. Mit steigendem B-Gehalt verändert sich das Kristallisationsverhalten.
Der mikrostrukturelle Werdegang während des Temperns von amorphem $Fe_{64}Cr_{18}Zr_8B_{10}$ wurde mit Hilfe einer Kombination aus Transmissions-Elektronenmikroskopie und energiedispersiver Röntgenmikroanalyse untersucht. Ein isothermes Tempern über zwei Stunden hinweg bei einer Temperatur zwischen 600 und 1000°C erzeugt eine Reihe von verschiedenen Mikrostrukturen - je nach Temperungstemperatur. Bei 600°C kristallisiert die amorphe Legierung partiell und

bildet eine Mikrostruktur, die aus 9 nm großen bcc Ferritkörnern, eingebettet in einer amorphen Matrix, besteht. Bei Temperaturen im Bereich von 700–900°C wandelt sich die Mikrostruktur der Legierung in ein Gemisch aus bcc Ferrit, defekten fcc MB_{12} Boridpartikeln und tetragonalen M_3B Boridpartikeln um. Bei 1000°C werden die defekten fcc MB_{12} Boridpartikel durch rhombische M_4B Boridpartikel ersetzt.